Improved protein contact prediction using dimensional hybrid residual networks and singularity enhanced loss function

Yunda Si and Chengfei Yan*

School of Physics, Huazhong University of Science and Technology, China

* Email: chengfeiyan@hust.edu.cn; Phone: +86-15337263247

Abstract

Deep residual learning has shown great success in protein contact prediction. In this study, a new deep residual learning-based protein contact prediction model was developed. Comparing with previous models, a new type of residual block hybridizing 1D and 2D convolutions was designed to increase the effective receptive field of the residual network, and a new loss function emphasizing the easily misclassified residue pairs was proposed to enhance the model training. The developed protein contact prediction model referred to as DRN-1D2D was first evaluated on 105 CASP 11 targets, 76 CAMEO hard targets and 398 membrane proteins together with two in house-developed reference models based on either the standard 2D residual block or the traditional BCE loss function, from which we confirmed that both the dimensional hybrid residual block and the singularity enhanced loss function can be employed to improve the model performance for protein contact prediction. DRN-1D2D was further evaluated on 39 CASP 13 and CASP 14 free modeling targets together with the two reference models and four state-of-the-art protein contact prediction models including DeepCov, DeepCon, RaptorX-Contact and TripleRes. The result shows that DRN-1D2D consistently achieved the best performance among all these models.

Key words: protein contact prediction, deep learning, residual network, receptive field, loss function

1 Introduction

The knowledge of protein residue-residue contacts is valuable for predicting protein structures with no-homologous templates, therefore, protein contact prediction had become a long-standing scientific problem for decades [1]. In recent years, great progress has been made on solving this problem due to the development of coevolutionary analysis methods and deep learning methods to predict protein contacts [2,3]. Coevolutionary analysis methods generally predict protein contacts through inferring residue pairs with direct evolutionary couplings from the multiple sequence alignment (MSA) of homologous proteins [4–8]. However, coevolutionary analysis methods can only accurately predict protein contacts when a large number of homologous sequences of the protein are available to produce an accurate estimation of the unknown parameters of the statistical models used in coevolutionary analysis. Deep learning methods apply deep learning models trained from large datasets of proteins to predict protein contacts, in which the coevolution and other properties of the protein obtained from the MSA of homologous proteins are often used as the input features. Deep learning methods are less dependent on the number of homologous sequences because parameters of the deep learning models are predetermined on large datasets of proteins.

Almost all top protein contact prediction models in recent Critical Assessment of protein Structure Prediction (CASP) are based on deep residual learning [2]. These models generally employ blocks of skip connected convolutional layers (residual blocks) to build the deep learning networks, and the parameters of the networks are determined through minimizing the loss between the predicted protein contact maps and the real protein contact maps in the training set. The first deep residual learning-based protein contact prediction method was developed by Xu and his coworkers, in which two residual networks were successively applied to transform the input features for protein contact prediction [9]. The first is a 1D residual network built by 1D residual blocks to conduct 1D convolutional transformations of the 1D sequential input features; the second is a 2D residual network built by 2D residual blocks to conduct 2D

convolutional transformations of the 2D pairwise features and the 2D transformed feature maps of the 1D sequential feature maps output from the 1D residual network. After Xu's work, deep residual learning was also applied by other groups to develop protein contact prediction models, in which efforts on improving the model performance include using much deeper residual networks, increasing the size of the training dataset, engineering new input features, employing metagenome sequence data and etc [10–16]. Most of these models only employed 2D residual blocks to build the residual network, in which the 2D transformed 1D sequential features were directly combined with the 2D pairwise features to form the input features of the residual network, or only the 2D pairwise features were used as the input features considering the pairwise features are generally much more important than the sequential features. It is clear that residual networks built by 2D residual blocks are effective network architectures for protein contact prediction, but whether the model performance can be further improved by designing novel residual blocks is unknown. Besides, appropriately calculating the training loss is also important for the model training. Most previous works applied the binary cross entropy (BCE) loss function to calculate the training loss, in which residue pairs in the protein contact map are equally weighted in the loss calculation. However, residue pairs in the contact-sparser regions (e.g. long-range contacts) of the protein contact map are more difficult to be correctly classified, emphasizing the easily misclassified residue pairs may enhance the model training.

In this study, we present a new deep residual learning-based protein contact prediction method. Comparing with previous models, a new type of residual block hybridizing 1D and 2D convolutions was designed to build the residual network, with which we show that the effective receptive field of the residual network can be significantly increased. Besides, a new loss function emphasizing the easily misclassified residue pairs was proposed to enhance the model training. The model was trained on the Xu's original training dataset [9] for developing the first deep residual learning-based protein contact method, which is referred to as DRN-1D2D in this study. Besides, we also developed two additional models

on the same dataset as the reference, in which one model was based on the basic 2D residual block and the BCE loss function, and another was based on the dimensional hybrid residual block and the BCE loss function. We first evaluated DRN-1D2D and the two reference models on Xu's original three test sets (105 CASP11 proteins, 76 CAMEO hard targets and 396 membrane proteins) [9]. The result shows that DRN-1D2D consistently outperformed the two reference models, and between the two reference models, the model based on the new residual block consistently outperformed the model based on the basic 2D residual block, which confirms that the dimensional hybrid residual block and the singularity enhanced loss function can both be employed to improve the model performance for protein contact prediction. Besides, DRN-1D2D also consistently outperformed Xu' original model, although these two models were developed on the same dataset and also have the same input features. We further evaluated DRN-1D2D on 39 CASP 13 and CASP 14 free modeling targets together with the two in house-developed reference models and four state-of-the-art protein contact prediction models including RaptorX-Contact [17], TripleRes [18], DeepCon [15] and DeepCov [10]. The result illustrates that DRN-1D2D consistently achieved the best performance among these models. It is worth noting that comparing with DRN-1D2D, both RaptorX-Contact and TripleRes have much larger network sizes and were also trained on much larger protein datasets.

2 Materials and methods

2.1 The network architecture of DRN-1D2D

2.1.1 The input feature maps

The input features of DRN-1D2D include three 1D sequential features: the position-specific scoring matrix (PSSM), the predicted 3-state secondary structure matrix (SS3), and the predicted 3-state solvent accessibility matrix (ACC), and four 2D pairwise features: the evolutionary coupling matrix from CCMpred [19], the mutual information matrix, the APC-corrected mutual information matrix and pairwise contact

potentials matrix, which are the same with Xu's original model [9]. The 1D sequential features are first concatenated along the columns. Let V = $\{v_1, v_2, \ldots, v_i, \ldots, v_L\}$ be the concatenated 1D sequential feature matrix where L is the sequence length and v_i is a vector storing the 1D features for residue i. A feature vector for residue pair ij can be created by concatenating v_{i}, $v_{(\mathrm{i+j})/2}$ and v_{j} to a single vector, with which we can convert the 1D sequential feature matrix to 2D pairwise feature maps. The 2D converted feature maps (L*L*78) of the 1D sequential features and the 2D pairwise feature maps (L*L*4) are further concatenated to form the input feature maps (L*L*82) of the network of DRN-1D2D.

2.1.2 The residual network

The network architecture of DRN-1D2D is shown in Figure 1A. First, a 1*1 convolutional layer followed by an instance normalization (IN) layer and a LeakyReLU activation layer is used to transform the number of channels of the input feature maps from 82 to 64. Then 25 residual blocks are used to transform the 64 channels of feature maps. Finally, another 1*1 convolutional layer is applied to transform the number of channels from 64 to 1, which is followed by the sigmoid transformation to produce the predicted contact map. In this study, instead of the 2D residual blocks, a new type of residual block hybridizing 1D and 2D convolutions was designed to build the residual network, which is described in the following section.

2.1.3 The dimensional hybrid residual block

Receptive field is defined as the spatial extent of the inputs used in the calculation of an output unit, and the input region outside the receptive field of the output unit does not affect the output value of that unit. The receptive field size is a crucial issue for designing convolutional neural networks, for the receptive field of the network needs to be large enough to capture the complex information in the input feature maps. Luo et al. show that the effective area in the receptive field only occupies a fraction of the theoretical receptive field, for the distribution of impact in the receptive field of 2D convolutional neural networks distributes as a gaussian, which generally decays quickly from the center [20]. In this study, to

increase the effective receptive field of the residual network, two additional 1D convolutional branches with kernel sizes of 9*1 and 1*9 are added to the basic 2D residual block formed by 3*3 convolution kernels (see Figure 1B and 1C, referred to as 2D block and 1D2D block in this study). Specifically, given an input of the residual block (x_i), the input is first transformed successively by the first convolution followed by instance normalization and LeakyReLU activation, and the second convolution followed by instance normalization from each branch separately; then the outputs from the three branches are summed together and added to the input ($x_i + f_{1*9}(x_i) + f_{3*3}(x_i) + f_{9*1}(x_i)$), which is finally transformed by the LeakyReLU activation to produce the output of the residual block. The dimensions of the input feature maps are kept in the convolutions through the application of zero paddings symmetrically on each feature map.

In Figure 2, we show the distribution of impact in the receptive field of the residual network built by 25 new residual blocks (i.e. the network of DRN-1D2D), by 25 basic 2D residual blocks, by 75 basic 2D residual blocks and by 142 basic 2D residual blocks respectively. The impact of each input pixel in the receptive field is evaluated by its input gradient when the convolution kernels are constant kernels. As we can see from Figure 2 that the residual network built by 25 new residual blocks has a much larger effective receptive field than the residual network built by 25 and 75 basic 2D residual blocks, and has a similar effective receptive field to the residual network built by 142 basic 2D residual blocks. The effective receptive field of the residual network built by 75 basic 2D residual blocks is shown as a reference for which has the same number of parameters with the network of DRN-1D2D (see Table S1).

2.2 The model training of DRN-1D2D

2.2.1 The calculation of training loss

Protein contact maps are sparse matrices in which contacting residue pairs are labeled with ones and non-contacting residue pairs are labeled with zeros. A pair of residues are generally considered to be in

contact if their C_β-C_β distance (C_α-C_α distance for GLY) is smaller than 8.0Å. A protein contact map generally contains much more zeros than ones, and regions that further away from the diagonal of the contact map is often sparser, for the residues separated by more residues have lower contact probabilities. Training a deep learning model for protein contact prediction is the process to determine the parameters of the network through minimizing the loss between the predicted protein contact maps and the real protein contact maps in the training set. In practice, due to the memory limitation, the parameters are usually updated successively based on the loss of each protein contact map (i.e. batch size equals to 1) across the training set, which is often calculated with the BCE loss function:

$$\mathrm{L}(\mathrm{y}, \hat{y}) = -\frac{1}{N}\sum_{|i-j|>5}\left[y_{ij} log \hat{y}_{ij} + (1 - y_{ij}) \log\left(1 - \hat{y}_{ij}\right)\right] \quad (1).$$

Where y represents the true contact map; $\hat{y}$ represents the prediction; N is the total number of the non-local residue pairs (residues separated by more than five residues). The local residue pairs are often not included in the loss calculation for the local residue contacts are trivially formed due to the peptide chain connection. In the BCE loss function, residue pairs in different regions of contact map are equally weighted. However, residue pairs in the contact-sparser regions (e.g. long-range contacts) of the protein contact map are more difficult to be correctly classified, therefore which should be emphasized in the model training. In this study, we propose a singularity enhanced loss function to increase the weight of these residue pairs:

$$\mathrm{L}(\mathrm{y}, \hat{y}) = -\sum_{|i-j|>5}\left[\alpha y_{ij} log \hat{y}_{ij} + (1 - \alpha)(1 - y_{ij}) \log\left(1 - \hat{y}_{ij}\right)\left(1 + \hat{y}_{ij}\right)^{\beta}\right] \quad (2).$$

Comparing with the BCE loss, first, a parameter α is introduced to weight the contacting and non-contacting residue pairs; second, $\left(1 + \hat{y}_{ij}\right)^{\beta}$ is introduced to increase the loss contribution from the misclassified non-contacting residue pairs. Since residue pairs in the contact-sparser regions of the contact map are more difficult to be correctly classified, the introduction of this term can automatically emphasize

these residue pairs. Besides, in the BCE loss, the mean of the losses across all non-local residue pairs are used in calculating the loss of each contact map, but in our proposed loss function, the sum rather than the mean is used to calculate the loss of each contact map, for we would like larger proteins to play a more important role in the model training. The two parameters α and β were carefully calibrated on a relative smaller dataset, and we found that when $\alpha = \frac{5}{6}$ and β=3, the obtained model achieved the best performance, therefore which were used in this study for the development of DRN-1D2D.

2.3.3 The training protocol

We trained the model of DRN-1D2D on the dataset of 6767 proteins prepared by Xu for developing the first deep residual learning-based protein contact prediction model [9]. Similar to Xu's protocol, seven different models were trained separately through seven-fold cross-validation from the dataset, and the final model is an average of the seven models. The He initialization [21] was used to initialize the parameters of the network, and the parameters were optimized by the AdamW optimizer with a weight decay of 0.1 and an initial learning rate of 0.001. In each epoch of training, the network parameters were successive updated based on the loss of each contact map across the training set calculated by the singularity enhanced loss function (i.e. batch size=1). If the total loss did not decrease within 2 epochs, the learning rate was decayed to 0.1 of its original value. After the learning rate decayed twice, the training was stopped, and the model with the lowest total loss from the previous epoch was saved as the final model for protein contact prediction (see Figure S1). The model was built with PyTorch and trained on the NVIDIA Tesla P100. Due to the GPU memory limitation, for the protein with sequence length larger than 400, a protein fragment with length equaling to 400 randomly selected from the protein was used in the model training. The average time for training a model is about 1 day. Besides, we also trained two additional models using the above protocol on the same dataset except that: in one model the residual blocks in the residual network were replaced by the basic 2D residual blocks and the training loss was

calculated by the BCE loss function; in another model, the dimensional hybrid residual network was kept but still the model was trained with the BCE loss. These two models referred to as BCE-2D and BCE-1D2D were used as the reference models in this study.

3. Results

3.1 The performance of DRN-1D2D on Xu's original three test sets

We first evaluated DRN-1D2D and the two reference models (BCE-2D and BCE-1D2D) on Xu's original three test sets (105 CASP 11 targets, 76 CAMEO targets and 398 membrane proteins), and the input features prepared by Xu were directly used by DRN-1D2D for protein contact prediction. In order to use the performance of Xu's original model as an extra reference, we used the same evaluation method as Xu to evaluate the performances of our models. Specifically, the accuracies of the top L/K (k=10, 5, 2, 1) of the short-, medium- and long-range predicted contacts were used to evaluate the performance of each model, where L is the protein sequence length [9]. A pair of residues are considered to be in contact if their C_β-C_β distance (C_α-C_α distance for GLY) is smaller than 8.0Å, and a contact is defined to be short-, medium- and long-range if the sequence distance of the two residues falls into [6, 11], [12, 23] and ≥ 24. In Table 1, we show the mean precisions of the contacts predicted by DRN-1D2D, the two reference models and Xu's original model on the three datasets. It is worth noting that the input features for all the four models are exactly the same. As we can see from Table 1, DRN-1D2D consistently outperformed all other models, and between the two reference models, the model based on the new residual block achieved better performances than the model based on the basic 2D residual block. The accuracy comparisons between DRN-1D2D and the two reference models on the top L/2 and L/5 of the predicted long-range contacts for all individual targets from the three test sets are shown in Figure 3. As we can see from Figure 3 that the improvements actually occur consistently across most of the targets, which

confirms that both the dimensional hybrid residual block and the singularity enhanced loss function can be employed to improve the model performance for protein contact prediction.

3.2 The performance of DRN-1D2D on recent CASP targets

DRN-1D2D was further evaluated on recent CASP targets. Specifically, the free modeling targets of CASP13 and CASP14 with released native structures (24 targets from CASP 13 and 15 targets from CASP14) were used to evaluate the performance of DRN-1D2D. For each target, we applied DeepMSA [22] to successively search Uniclust30 (2018-08) [23], Uniref90 (2019-11) [24] and Metaclust (2018-06) [25] to build the MSA of its homologous proteins, from which we extract the input features for DRN-1D2D according to the protocols described by Xu [9]. Besides, the two in-house developed reference models and four state-of-the-art protein contact prediction models including DeepCov, DeepCon, RaptorX-Contact and TripleRes were also applied to predict the protein contacts on the same dataset. To ensure a fair comparison, for each target, the input features of all the above models were extracted from the same MSA. The performance of each model was evaluated by calculating the accuracies of the top L/K (K=5, 2, 1) of the medium + long-range (sequence distance≥ 12) and long-range (sequence distance≥ 24) of the predicted contacts, which is the same with the recent CASP protocol for evaluating the performance of protein contact prediction[2]. In Table 2, we show the mean precisions of the contacts predicted by these models on the CASP13 and CASP14 targets respectively. As we can see from Table 2 that DRN-1D2D consistently achieved the best performances on both CASP 13 and CASP 14 targets. Besides, the accuracy comparisons between DRN-1D2D and other models on the top L/5 of the predicted long-range, medium + long-range contacts for all individual targets are shown in Figure 4 (Figure 4A-4B: DRN-1D2D versus the two in house-developed reference models; Figure 4C-4D: DRN-1D2D versus the four state-of-the-art models; for the top L/2 contact prediction, see Figure S2). As we can see from Figure 4 that DRN-1D2D consistently outperforms other models for most of the targets. It is worth noting that RaptorX-Contact is a new version of Xu's original protein contact prediction model, which was trained on a much larger

dataset containing 11410 proteins, and has a much larger network architecture; the network architecture of TripleRes is formed by four residual networks, each of the residual network has a network depth similar to DRN-1D2D [17,18].

3.3 The impact of MSA on the model performance of DRN-1D2D

We analyzed the impact of MSA on the model performance of DRN-1D2D. Specifically, for each target, the normalized effective sequence number of the MSA (N_{eff}^{norm}) was calculated according to:

$$N_{eff}^{norm}=\frac{1}{\sqrt{L}}\sum_{n=1}^{N}\frac{1}{m_n} \quad (3).$$

Where N is the total number of sequences in the MSA; $\frac{1}{m_n}$ is the weight the n-th sequence with m_n being the number of sequences in the MSA which have a sequence identity higher than 80% to the n-th sequence; L is the sequence length. In Figure 5, we show the accuracy of the top L/5 long range predicted contacts from DRN-1D2D versus N_{eff}^{norm} for each individual target (see Figure S3 for other models). As we can see from Figure 5, the accuracy of the contact prediction yields a modest correlation with N_{eff}^{norm}, in which targets with higher N_{eff}^{norm} tend to have higher contact prediction accuracies. However, for about 60% (13/22) of the targets with very low N_{eff}^{norm} ($N_{eff}^{norm} \leq 10$), the top L/5 long range contacts predicted by DRN-1D2D still have an accuracy higher than 50%.

We further grouped the targets into two groups according to the value of N_{eff}^{norm} (low N_{eff}^{norm} group: $N_{eff}^{norm} \leq 10$; high N_{eff}^{norm} group: $N_{eff}^{norm} > 10$), and analyzed the performances of DRN-1D2D and other models on the two groups of targets respectively. In Figure 6, we show the mean precisions of the top L/5 and top L/2 of the medium + long range (Figure 6A) and long range (Figure 6B) contacts predicted by each model on the two groups of targets. As we can see from Figure 6, for both the two groups, DRN-1D2D consistently achieved the best performances among these models. Besides, if DeepCov is considered as the base model, the performance improvement of DRN-1D2D on the low N_{eff}^{norm} group is much higher

than that on the high N_{eff}^{norm}, which illustrates that DRN-1D2D has a lower dependency on the number of sequences in the MSA.

4 Discussion and Conclusion

A new deep residual learning-based protein contact prediction model referred to as DRN-1D2D was presented in this study. Different from previous models, a new type of residual block hybridizing 1D and 2D convolutions was applied to build the residual network of DRN-1D2D, with which we show the effective receptive field of the residual network can be significantly increased, and a new loss function emphasizing the easily misclassified residue pairs was applied to enhance the model training. We first evaluated DRN-1D2D on Xu's original three test sets together with two in house-developed reference models: one based on the basic 2D residual block and the BCE loss function, and another based on the dimensional hybrid residual block and the BCE loss function. Besides, Xu's original model performance was also used as a reference. The result shows that DRN-1D2D consistently outperforms the two reference models and Xu's original model. Between the two reference models, the model based on the new residual block consistently outperforms the basic 2D residual block, which confirms that the introduction of the dimensional hybrid residual block and the singularity enhanced loss function are effective protocols to improve the model performance for protein contact prediction. We further evaluated DRN-1D2D on recent CASP targets together with the two reference models and four state-of-the-art protein contact prediction models including DeepCov, DeepCon, RaptorX-Contact and TripleRes. The result shows that DRN-1D2D achieved the best performance among these models, although DRN-1D2D was trained on a relative older and smaller dataset and has a much smaller network architecture than RaptorX-Contact and TripleRes. It is reasonable to assume our model can be further improved if we can build a deeper residual network with more residual blocks and train the model on larger training sets. In this study, the depth of our residual network was limited by the GPU memory. Besides, we also

analyzed the impact of the MSA on the model performance, which shows that the accuracy of the predicted contacts has a moderate correlation with the normalized effective sequence number of the MSA (i. e. N_{eff}^{norm}). However, even when N_{eff}^{norm} is very low ($N_{eff}^{norm} < 10$), DRN-1D2D still produced accurate contact predictions for 60% of the targets, which illustrates the robustness of DRN-1D2D.

Availability

DRN-1D2D is available at https://github.com/ChengfeiYan/DRN-1D2D.

Funding

This work is supported by the startup grant of Huazhong University of Science and Technology.

Reference

1. Kuhlman B, Bradley P. Advances in protein structure prediction and design. Nat. Rev. Mol. Cell Biol. 2019; 20:681–697

2. Shrestha R, Fajardo E, Gil N, et al. Assessing the accuracy of contact predictions in CASP13. Proteins Struct. Funct. Bioinforma. 2019; 87:

3. Wuyun Q, Zheng W, Peng Z, et al. A large-scale comparative assessment of methods for residue–residue contact prediction. Brief. Bioinform. 2018; 19:

4. Morcos F, Pagnani A, Lunt B, et al. Direct-coupling analysis of residue coevolution captures native contacts across many protein families. Proc. Natl. Acad. Sci. 2011; 108:E1293 LP-E1301

5. Kamisetty H, Ovchinnikov S, Baker D. Assessing the utility of coevolution-based residue–residue contact predictions in a sequence- and structure-rich era. Proc. Natl. Acad. Sci. 2013; 110:15674 LP – 15679

6. de Juan D, Pazos F, Valencia A. Emerging methods in protein co-evolution. Nat. Rev. Genet. 2013; 14:249–261

7. Ovchinnikov S, Kinch L, Park H, et al. Large-scale determination of previously unsolved protein structures using evolutionary information. Elife 2015; 4:e09248

8. Ovchinnikov S, Park H, Varghese N, et al. Protein structure determination using metagenome sequence data. Science (80-.). 2017; 355:

9. Wang S, Sun S, Li Z, et al. Accurate De Novo Prediction of Protein Contact Map by Ultra-Deep Learning Model. PLOS Comput. Biol. 2017; 13:e1005324

10. Jones DT, Kandathil SM. High precision in protein contact prediction using fully convolutional neural networks and minimal sequence features. Bioinformatics 2018; 34:3308–3315

11. Hanson J, Paliwal K, Litfin T, et al. Accurate prediction of protein contact maps by coupling residual two-dimensional bidirectional long short-term memory with convolutional neural networks. Bioinformatics 2018; 34:

12. Li Y, Hu J, Zhang C, et al. ResPRE: High-accuracy protein contact prediction by coupling precision matrix with deep residual neural networks. Bioinformatics 2019; 35:

13. Wu Q, Peng Z, Anishchenko I, et al. Protein contact prediction using metagenome sequence data and residual neural networks. Bioinformatics 2020;

14. Li Y, Zhang C, Bell EW, et al. Deducing high-accuracy protein contact-maps from a triplet of coevolutionary matrices through deep residual convolutional networks. bioRxiv 2020;

15. Adhikari B. DEEPCON: Protein contact prediction using dilated convolutional neural networks with dropout. Bioinformatics 2020; 36:

16. Chen C, Wu T, Guo Z, et al. Combination of deep neural network with attention mechanism enhances the explainability of protein contact prediction. Proteins Struct. Funct. Bioinforma. 2021;

17. Xu J. Distance-based protein folding powered by deep learning. Proc. Natl. Acad. Sci. U. S. A. 2019; 116:

18. Li Y, Zhang C, Bell EW, et al. Deducing high-accuracy protein contact-maps from a triplet of coevolutionary matrices through deep residual convolutional networks. PLOS Comput. Biol. 2021; 17:

19. Seemayer S, Gruber M, Söding J. CCMpred—fast and precise prediction of protein residue–residue contacts from correlated mutations. Bioinformatics 2014; 30:3128–3130

20. Luo W, Li Y, Urtasun R, et al. Understanding the effective receptive field in deep convolutional neural networks. Adv. Neural Inf. Process. Syst. 2016;

21. He K, Zhang X, Ren S, et al. Delving Deep into Rectifiers: Surpassing Human-Level Performance on ImageNet Classification. Proc. 2015 IEEE Int. Conf. Comput. Vis. 2015; 1026–1034

22. Zhang C, Zheng W, Mortuza SM, et al. DeepMSA: constructing deep multiple sequence alignment to improve contact prediction and fold-recognition for distant-homology proteins. Bioinformatics 2020; 36:2105–2112

23. Mirdita M, von den Driesch L, Galiez C, et al. Uniclust databases of clustered and deeply annotated protein sequences and alignments. Nucleic Acids Res. 2017; 45:D170–D176

24. Suzek BE, Huang H, McGarvey P, et al. UniRef: comprehensive and non-redundant UniProt reference clusters. Bioinformatics 2007; 23:1282–1288

25. Steinegger M, Söding J. Clustering huge protein sequence sets in linear time. Nat. Commun. 2018; 9:2542

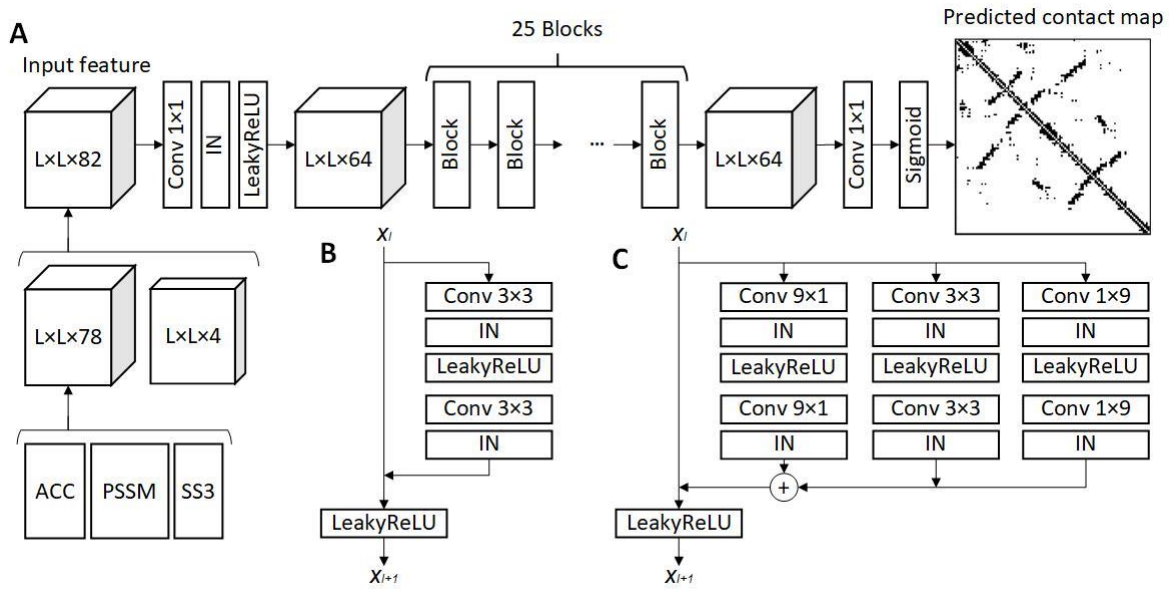

Figure 1. The network architecture of DRN-1D2D. (A) The overall architecture residual network. (B) The basic 2D residual block. (C) The dimensional hybrid residual block.

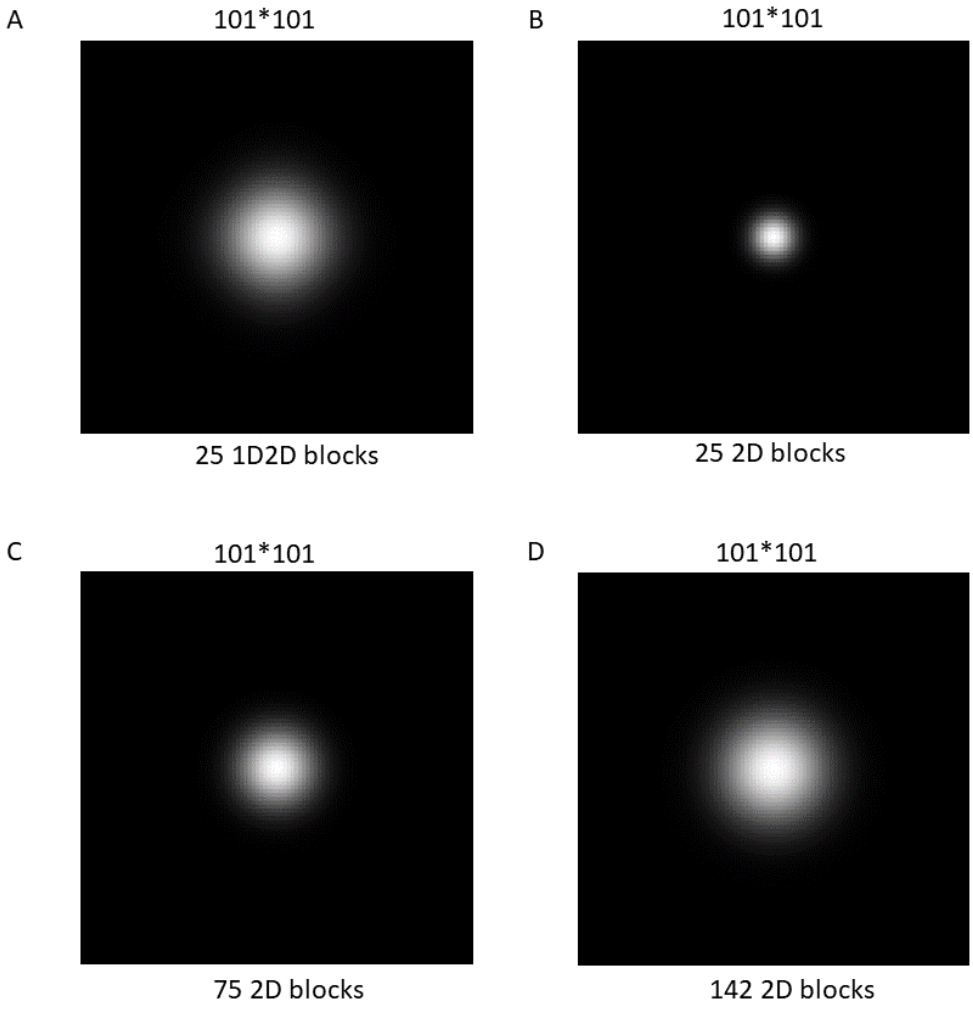

Figure 2. The distribution of impact in the receptive field of the residual network built by (A) 25 1D2D blocks; (B) 25 2D blocks; (C) 75 2D blocks; (D) 142 2D blocks.

Table 1. The mean precisions of contacts predicted by different models on Xu's original three test sets

Test sets	Method	Short				Medium				Long			
		L/10	L/5	L/2	L	L/10	L/5	L/2	L	L/10	L/5	L/2	L
CASP11	Xu 2017	0.82	0.70	0.46	0.28	0.85	0.76	0.55	0.35	0.81	0.77	0.68	0.55
	BCE-2D	0.83	0.72	0.47	0.29	0.83	0.75	0.55	0.36	0.79	0.77	0.66	0.54
	BCE-D2D	0.84	0.73	0.48	0.29	0.84	0.76	0.56	0.36	0.83	0.79	0.69	0.56
	DRN-1D2D	**0.86**	**0.75**	**0.49**	**0.29**	**0.86**	**0.78**	**0.58**	**0.37**	**0.86**	**0.82**	**0.73**	**0.59**
CAMEO	Xu 2017	0.67	0.57	0.37	0.23	0.69	0.61	0.42	0.28	0.69	0.65	0.55	0.42
	BCE-2D	0.69	0.59	0.41	0.25	0.68	0.60	0.44	0.30	0.67	0.63	0.53	0.41
	BCE-1D2D	0.72	0.60	0.41	0.25	0.72	0.63	0.46	0.30	0.69	0.65	0.55	0.43
	DRN-1D2D	**0.75**	**0.63**	**0.43**	**0.26**	**0.74**	**0.65**	**0.47**	**0.31**	**0.74**	**0.69**	**0.59**	**0.46**
Mems	Xu 2017	0.60	0.46	0.27	0.16	0.66	0.53	0.33	0.22	0.78	0.73	0.62	0.47
	BCE-2D	0.62	0.49	0.30	0.18	0.67	0.55	0.36	0.23	0.77	0.73	0.62	0.48
	BCE-1D2D	0.64	0.50	0.31	0.18	0.67	0.56	0.36	0.23	0.78	0.74	0.64	0.49
	DRN-1D2D	**0.65**	**0.52**	**0.32**	**0.19**	**0.70**	**0.58**	**0.38**	**0.24**	**0.81**	**0.77**	**0.67**	**0.53**

Note: The highest accuracy in each category is highlighted in bold font.

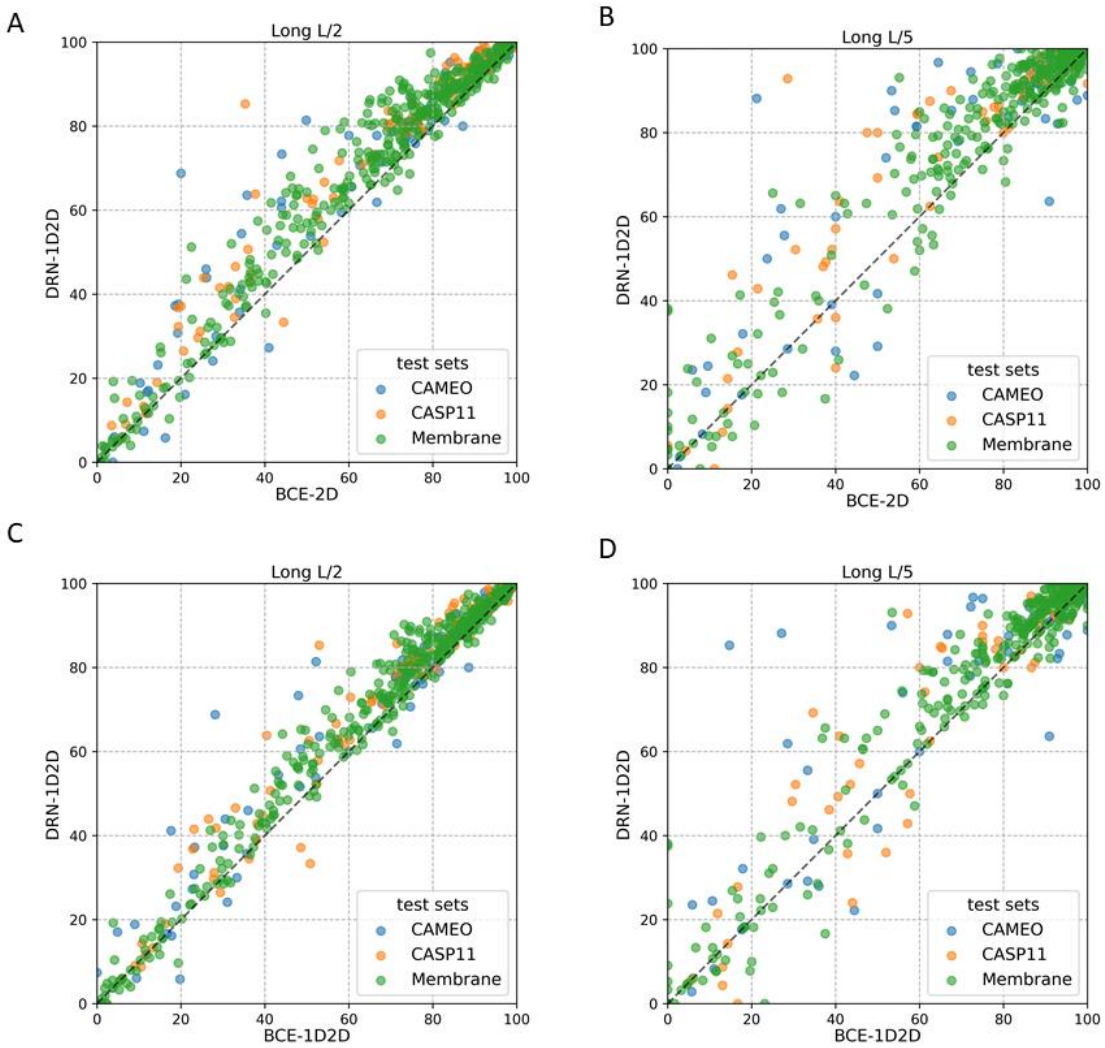

Figure 3. The performance comparison between DRN-1D2D and the two in house-developed reference models (BCE-2D and BCE-1D2D) for all individual targets from Xu's three original test sets. (A) DRN-1D2D versus BCE-2D for top L/2 long range predicted contacts. (B) DRN-1D2D versus BCE-2D for top L/5 long range predicted contacts. (C) DRN-1D2D versus BCE-1D2D for top L/2 long range predicted contacts. (D)DRN-1D2D versus BCE-1D2D for top L/5 long range predicted contacts.

Table 2. The mean precisions of contacts predicted by different models on CASP 13 and 14 targets

Method	CASP13						CASP14					
	Medium+Long			Long			Medium+Long			Long		
	L/5	L/2	L	L/5	L/2	L	L/5	L/2	L	L/5	L/2	L
DeepCov	0.69	0.58	0.46	0.53	0.43	0.33	0.35	0.27	0.21	0.25	0.19	0.15
DeepCon	0.81	0.70	0.56	0.64	0.54	0.42	0.44	0.37	0.28	0.31	0.24	0.18
BCE-2D	0.81	0.71	0.61	0.72	0.59	0.46	0.50	0.39	0.30	0.32	0.26	0.21
TripleRes	0.82	0.72	0.62	0.73	0.61	0.49	0.50	0.41	0.31	0.35	0.28	0.21
BCE-1D2D	0.82	0.72	0.62	0.72	0.61	0.49	0.52	0.42	0.33	0.39	0.30	0.21
RaptorX-Contact	0.81	0.75	0.62	0.73	0.62	0.49	0.53	0.42	0.32	0.36	0.29	0.22
DRN-1D2D	**0.88**	**0.79**	**0.67**	**0.77**	**0.66**	**0.52**	**0.58**	**0.46**	**0.36**	**0.46**	**0.33**	**0.24**

Note: The highest accuracy in each category is highlighted in bold font.

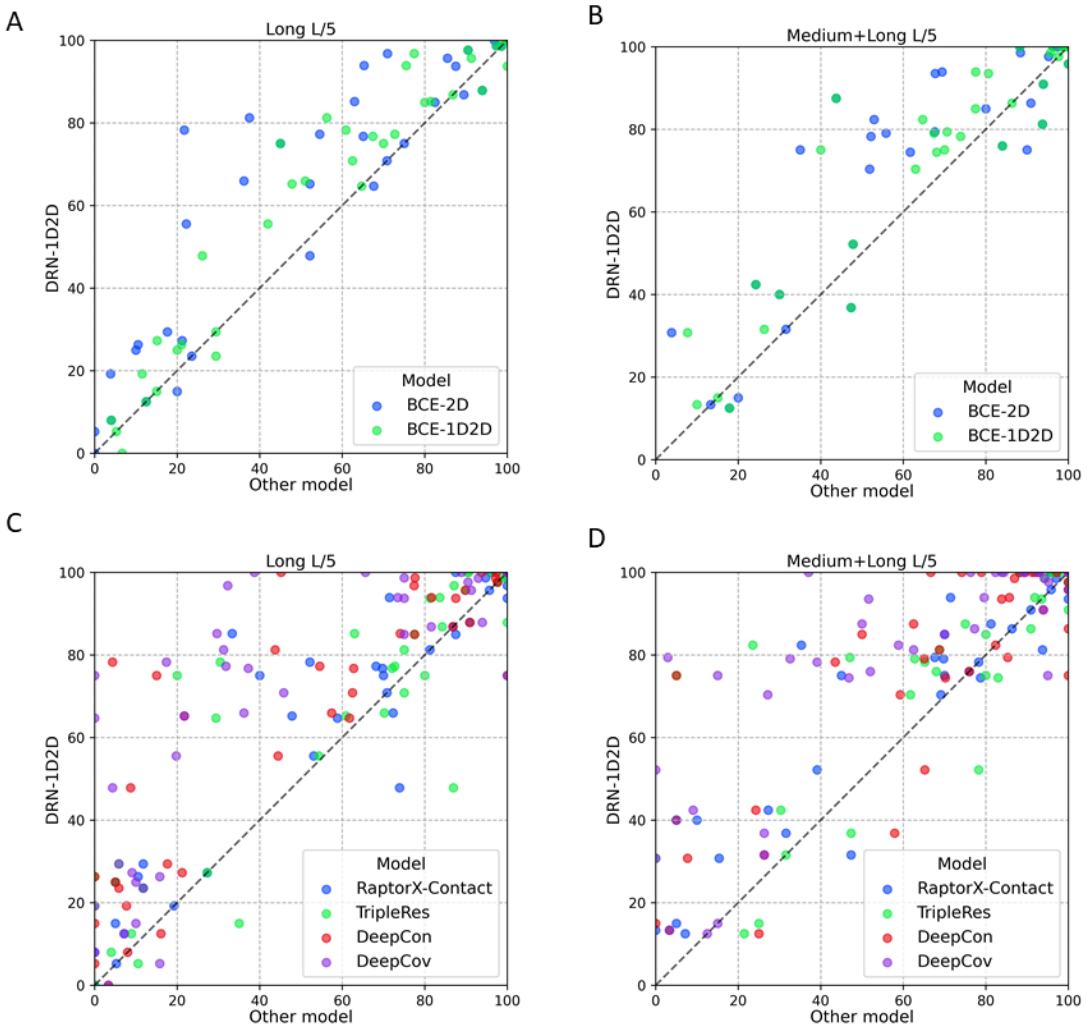

Figure 4. The performance comparison between DRN-1D2D and other models for all individual targets of the CASP 13 and 14 free modeling targets. (A) DRN-1D2D versus the two in house-developed reference models for top L/5 long range predicted contacts. (B) DRN-1D2D versus the two in house-developed reference models for top L/5 medium + long range predicted contacts (C) DRN-1D2D versus four state-of-the-art outside models for top L/5 long range predicted contacts. (D) DRN-1D2D versus four state-of-the-art outside models for top L/5 medium + long range predicted contacts.

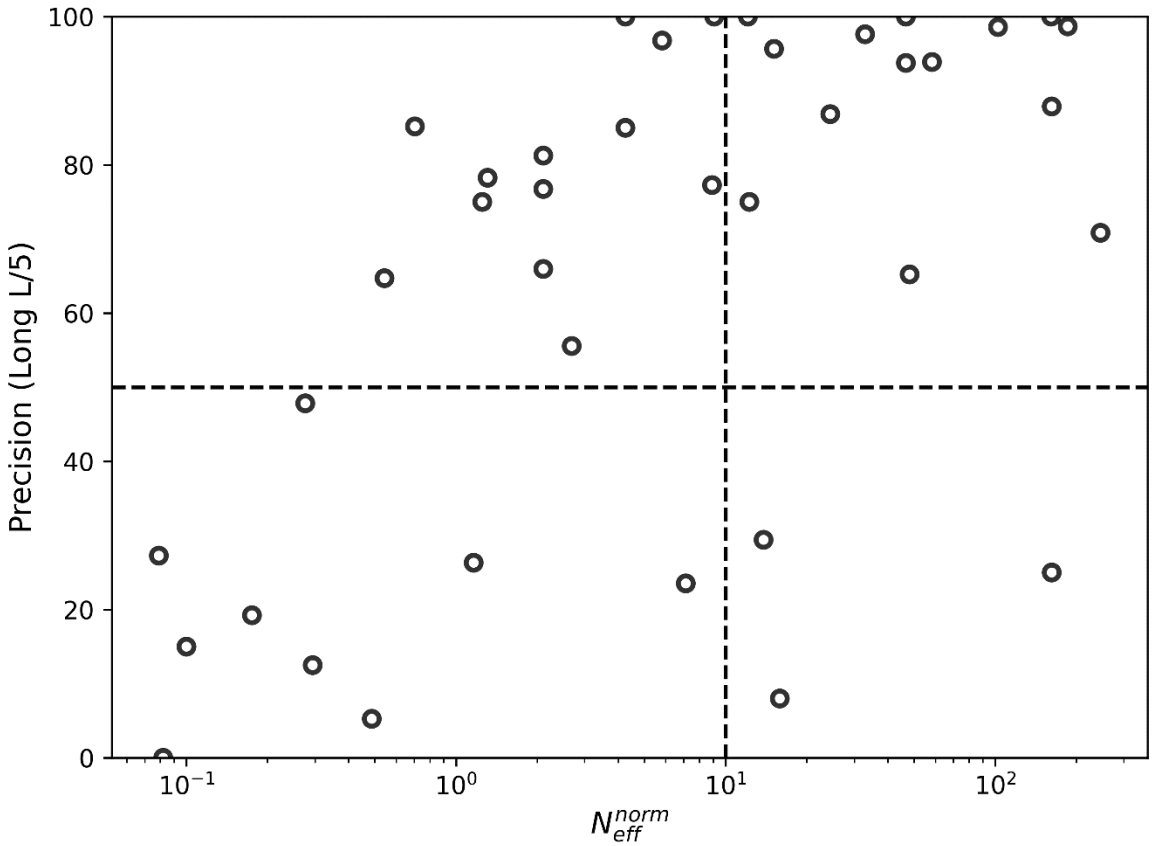

Figure 5. Precision of top L/5 long range predicted contacts by DRN-1D2D versus N_{eff}^{norm} of the MSA.

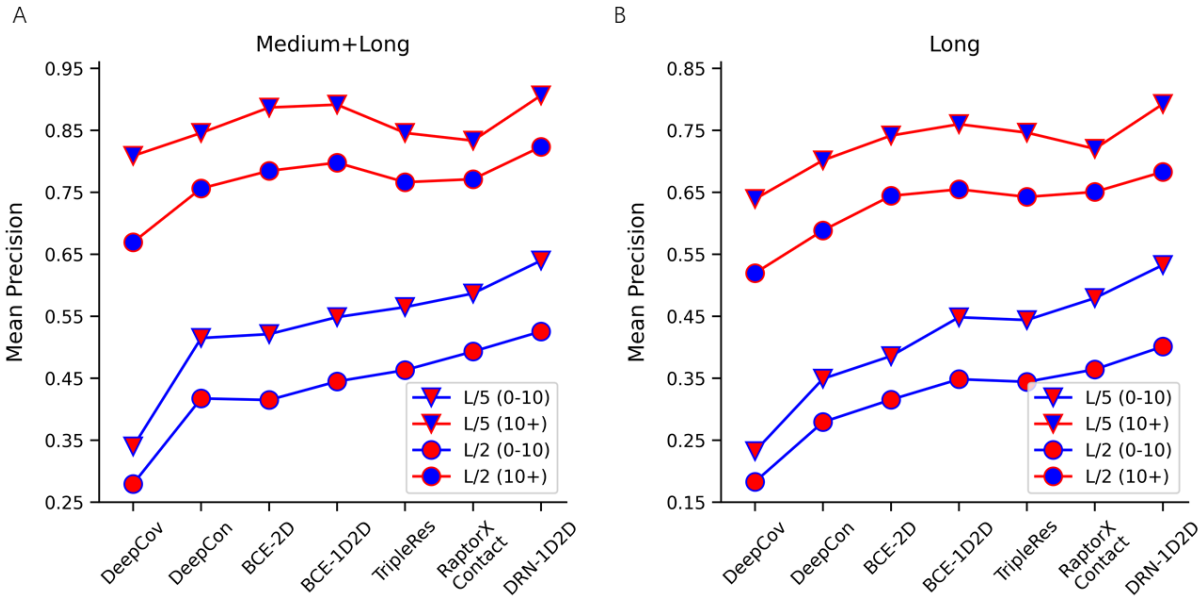

Figure 6. The mean precisions of the top L/5 and top L/2 of the medium + long-range and long-range contacts predicted by different models on two groups of targets with $N_{eff}^{norm} \leq 10$ and $N_{eff}^{norm} > 10$ respectively: (A) medium + long-range contact prediction; (B) long-range contact prediction.

Supplementary

Table S1. Parameter number and ERF comparison for residual networks formed by different numbers of 2D blocks and 1D2D blocks*

Block	2D Block			1D2D Block
# of blocks	25	75	142	25
Params	1	3	5.68	3
ERF	1	1.76	2.435	2.426

Note: The residual network formed by 25 2D blocks are used a reference. The ERF size of each residual network is evaluated by the full width at half maxima (FWHM) of the impact distribution. For example, the ERF of the residual network formed by 25 1D2D blocks has an FWHM 2.426 times larger than the residual network formed by the same number of 2D blocks.

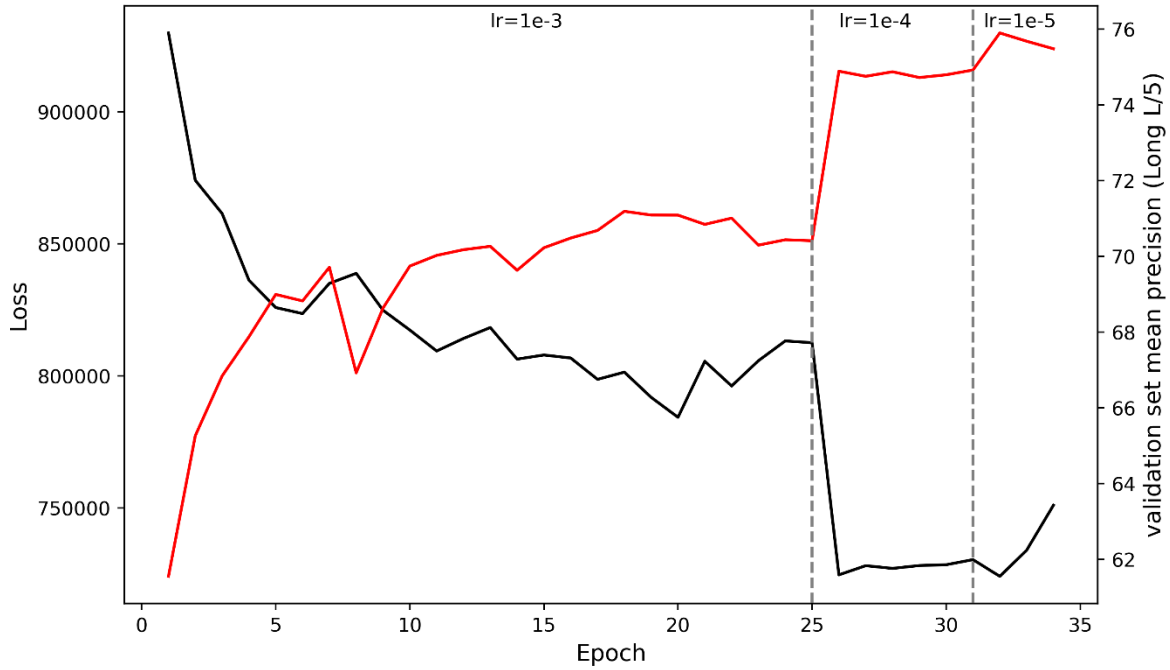

Figure S1. The change of training loss, validation accuracy and learning rate for a model training of DRN-1D2D.

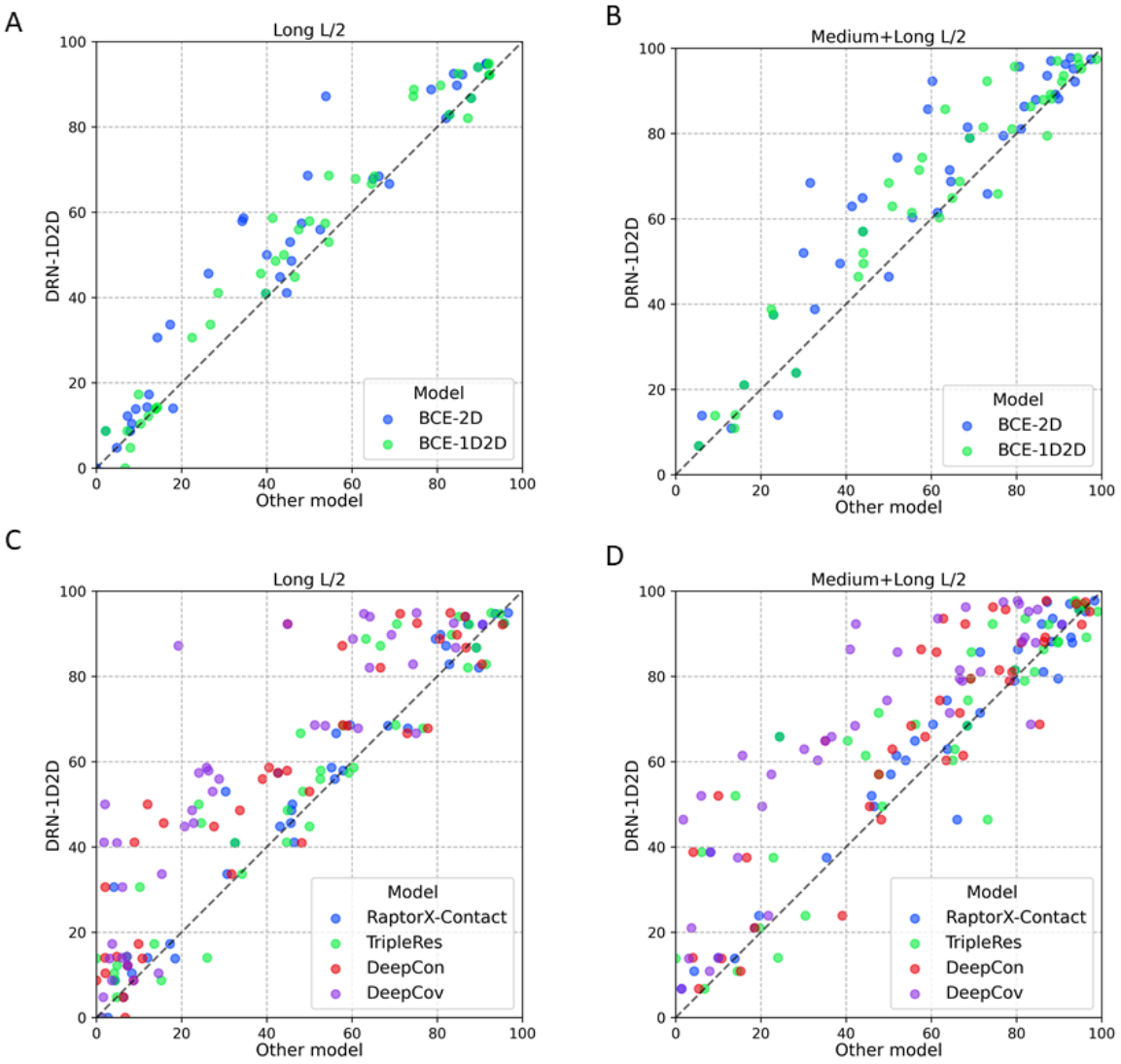

Figure S2. The performance comparison between DRN-1D2D and other models for all individual targets from the CASP datasets. (A) DRN-1D2D versus the two in house-developed reference models for top L/2 long range predicted contacts. (B) DRN-1D2D versus the two in house-developed reference models for top L/2 medium + long range predicted contacts (C) DRN-1D2D versus four state-of-the-art outside models for top L/2 long range predicted contacts. (D) DRN-1D2D versus four state-of-the-art outside models for top L/2 medium + long range predicted contacts.

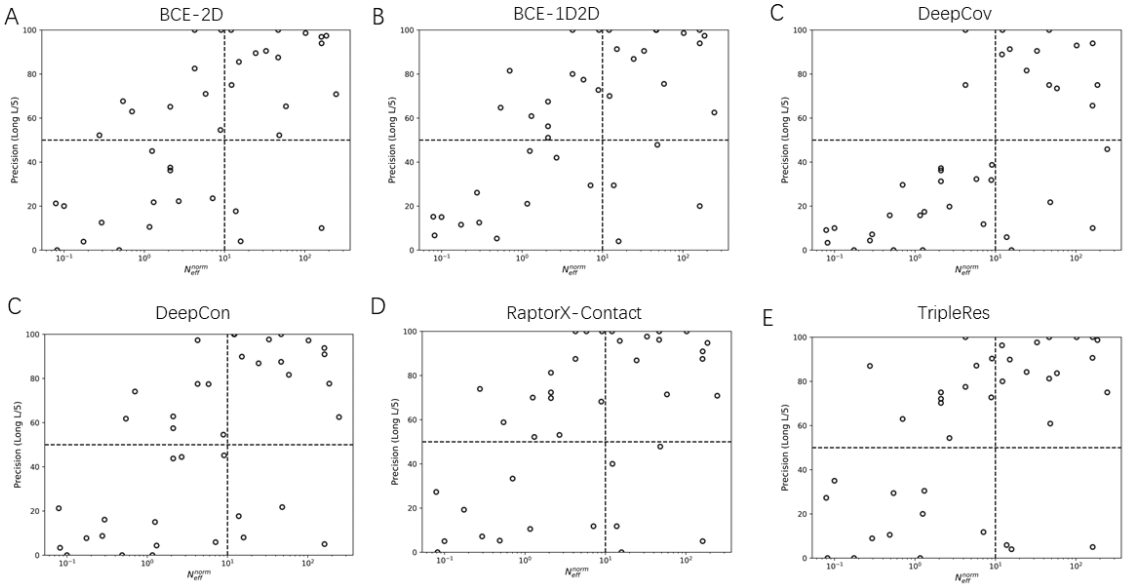

Figure S3. Precision of top L/5 long range predicted contacts versus N_{eff}^{norm} of MSAs for different models: (A) BCE-2D; (B) BCE-1D2D; (C) DeepCov; (D) DeepCon; (E) RaptorX-Contact; (F) TripleRes.

Data S1. The accuracy of protein contact prediction for each individual target from the CASP datasets.

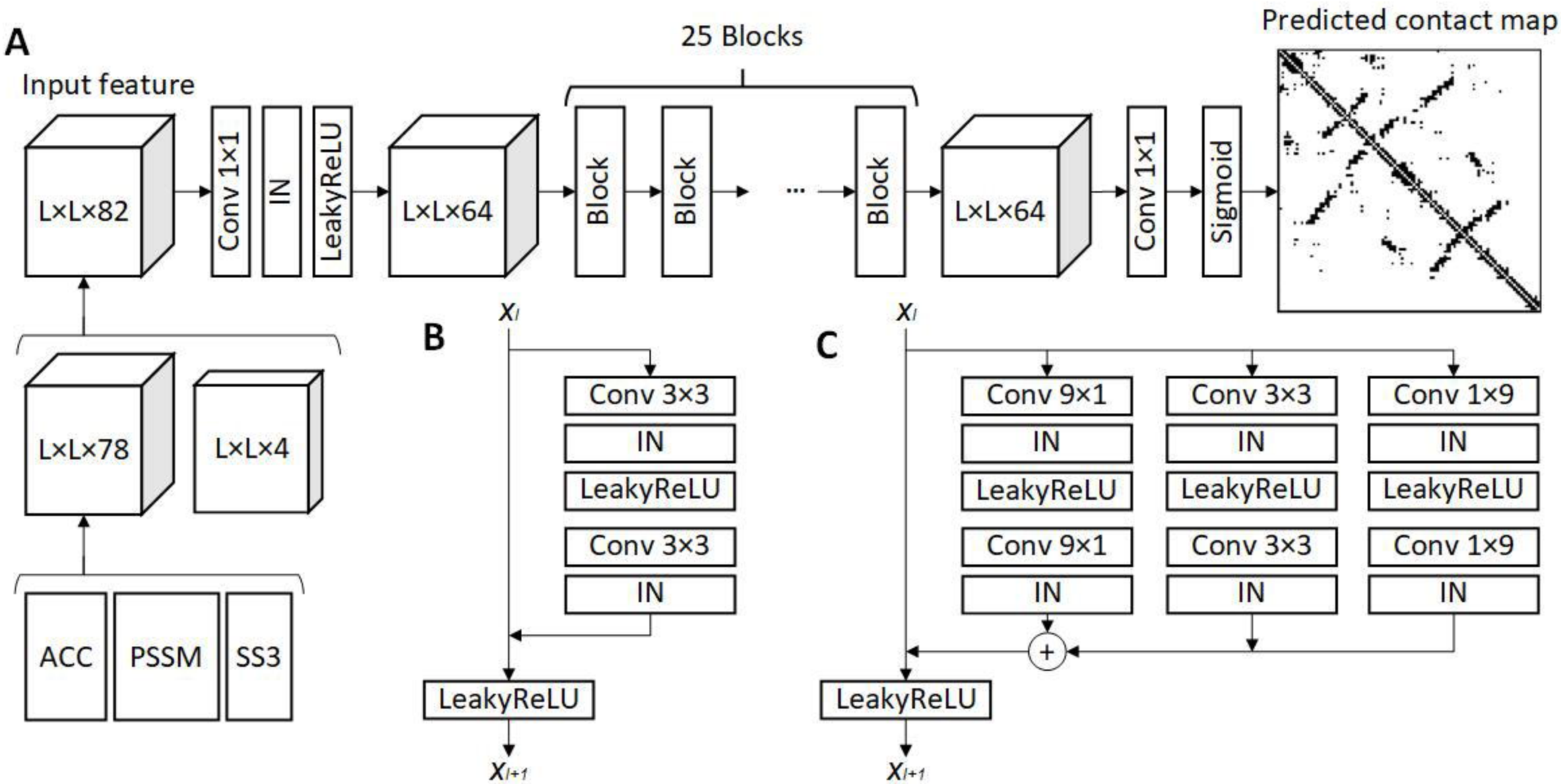
A
Input feature
25 Blocks
Predicted contact map
L×L×82
Conv 1×1
IN
LeakyReLU
L×L×64
Block
Block
Block
L×L×64
Conv 1×1
Sigmoid
L×L×78
L×L×4
ACC
PSSM
SS3
B
x_l
Conv 3×3
IN
LeakyReLU
Conv 3×3
IN
LeakyReLU
x_{l+1}
C
x_l
Conv 9×1
IN
LeakyReLU
Conv 9×1
IN
Conv 3×3
IN
LeakyReLU
Conv 3×3
IN
Conv 1×9
IN
LeakyReLU
Conv 1×9
IN
+
LeakyReLU
x_{l+1}

A

101*101

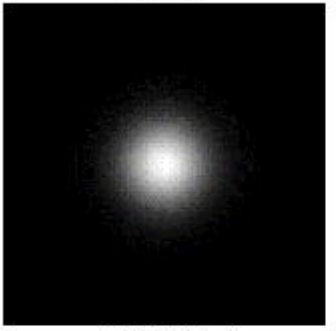

25 1D2D blocks

B

101*101

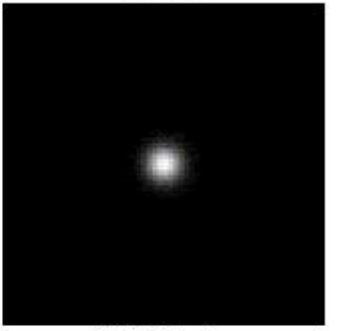

25 2D blocks

C

101*101

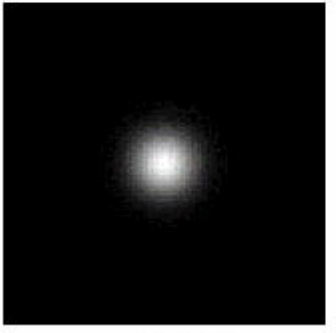

75 2D blocks

D

101*101

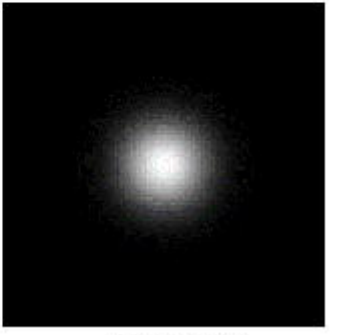

142 2D blocks

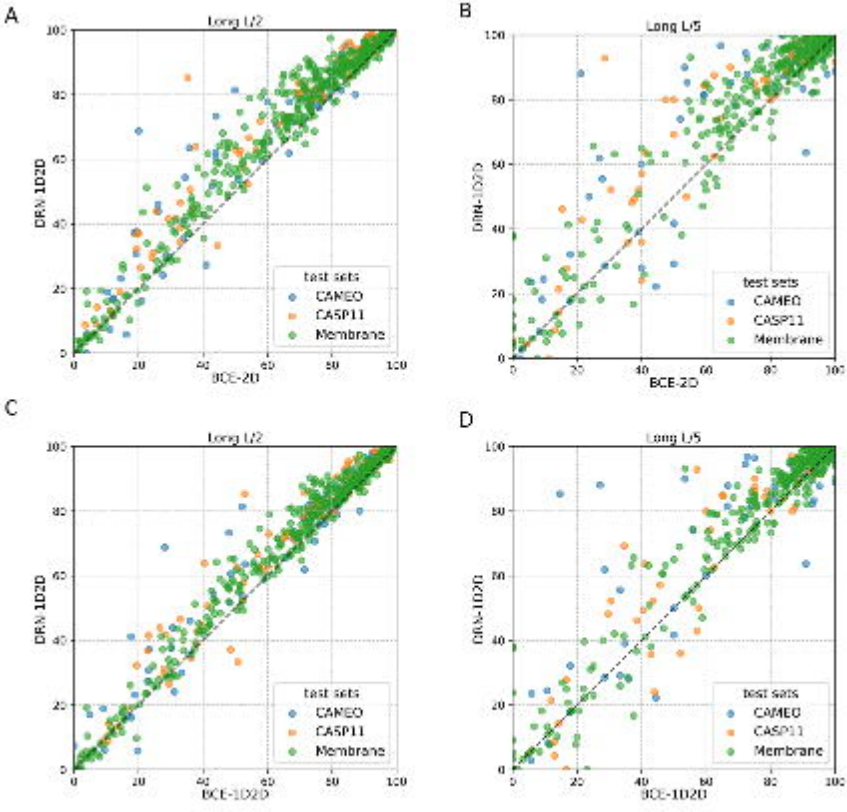
A
Long L/2
DRN-1D2D
BCE-2D
test sets
CAMEO
CASP11
Membrane
B
Long L/5
DRN-1D2D
BCE-2D
test sets
CAMEO
CASP11
Membrane
C
Long L/2
DRN-1D2D
BCE-1D2D
test sets
CAMEO
CASP11
Membrane
D
Long L/5
DRN-1D2D
BCE-1D2D
test sets
CAMEO
CASP11
Membrane

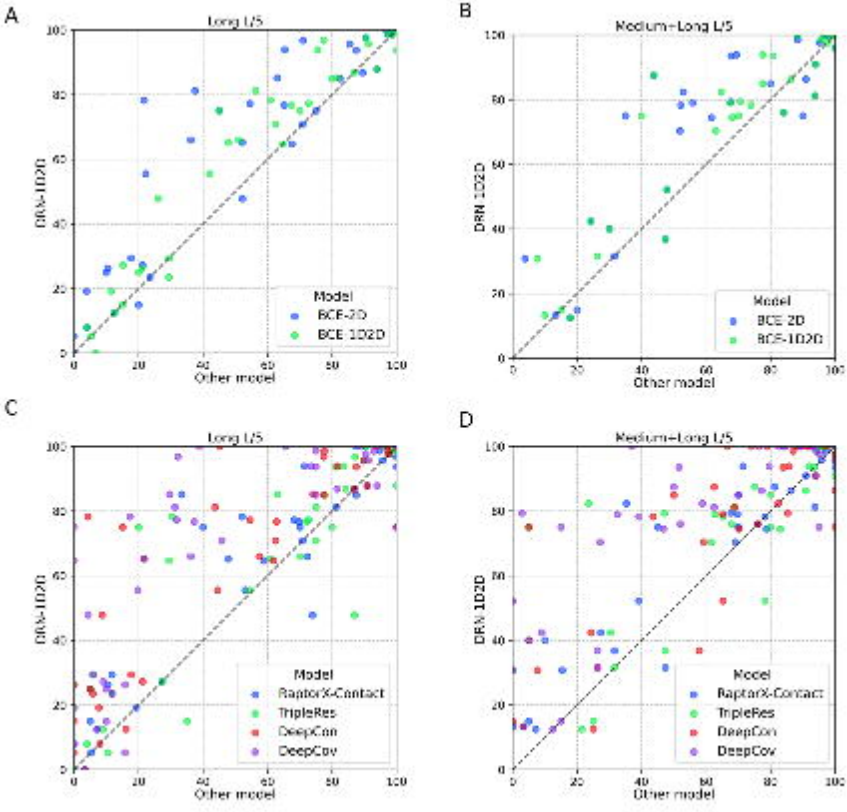
A
Long L/5
DRN-1D2D
Other model
Model
BCE-2D
BCE 1D2D
B
Medium+Long L/5
DRN 1D2D
Other model
Model
BCE 2D
BCE-1D2D
C
Long L/5
DRN-1D2D
Other model
Model
RaptorX-Contact
TripleRes
DeepCon
DeepCov
D
Medium+Long L/5
DRN 1D2D
Other model
Model
RaptorX-Contact
TripleRes
DeepCon
DeepCov

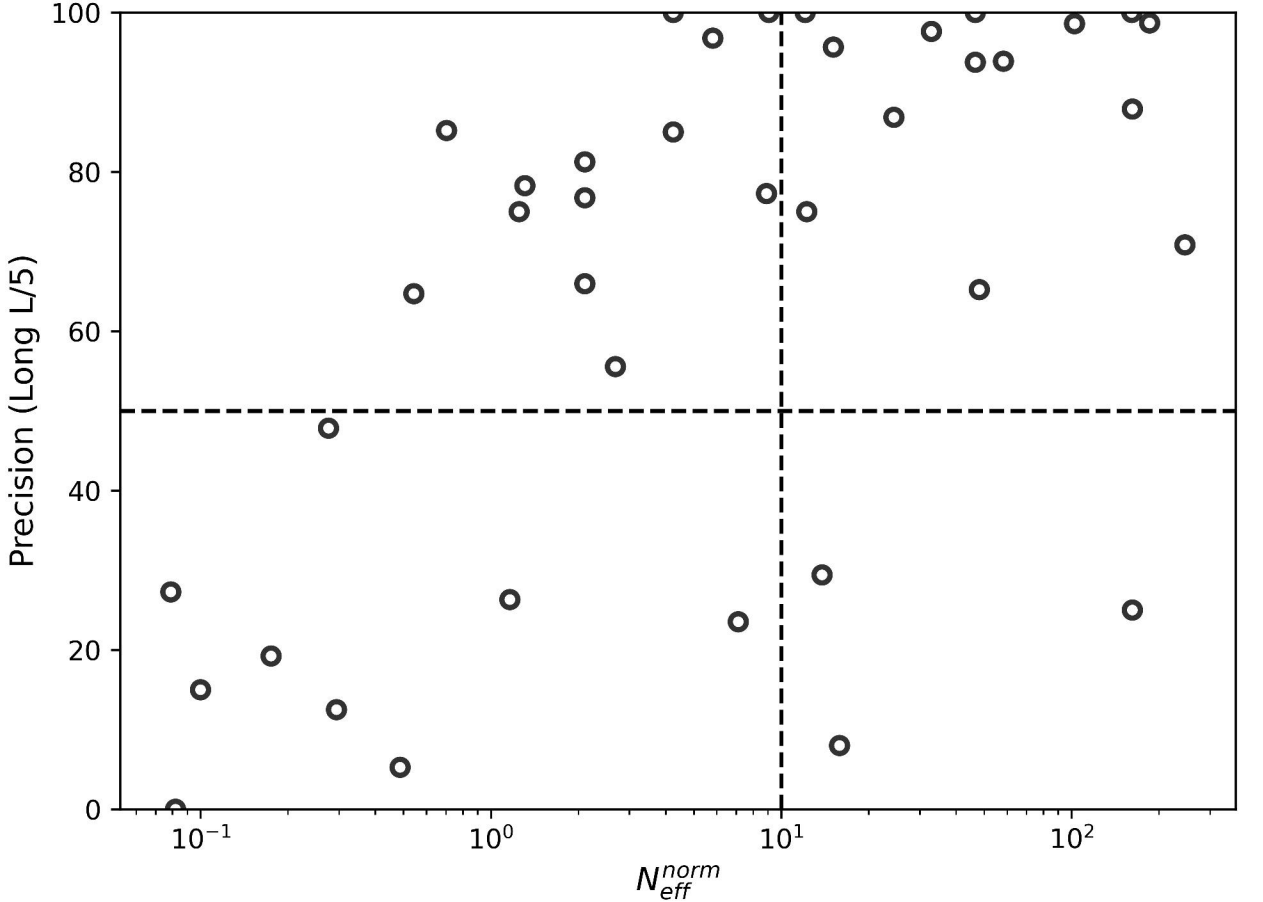
Precision (Long L/5)
100
80
60
40
20
0
10^{-1}
10^{0}
10^{1}
10^{2}
N_{eff}^{norm}

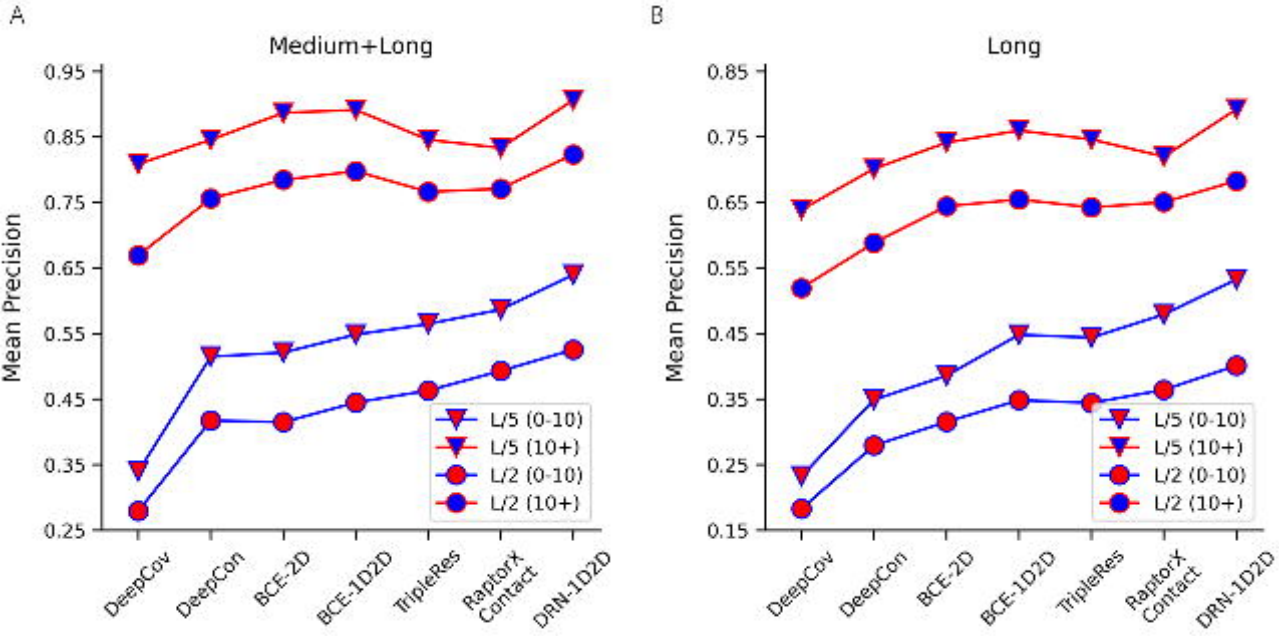
A
Medium+Long
Mean Precision
0.95
0.85
0.75
0.65
0.55
0.45
0.35
0.25
L/5 (0-10)
L/5 (10+)
L/2 (0-10)
L/2 (10+)
DeepCov
DeepCon
BCE-2D
BCE-1D2D
TripleRes
RaptorX Contact
DRN-1D2D
B
Long
Mean Precision
0.85
0.75
0.65
0.55
0.45
0.35
0.25
0.15
L/5 (0-10)
L/5 (10+)
L/2 (0-10)
L/2 (10+)
DeepCov
DeepCon
BCE-2D
BCE-1D2D
TripleRes
RaptorX Contact
DRN-1D2D

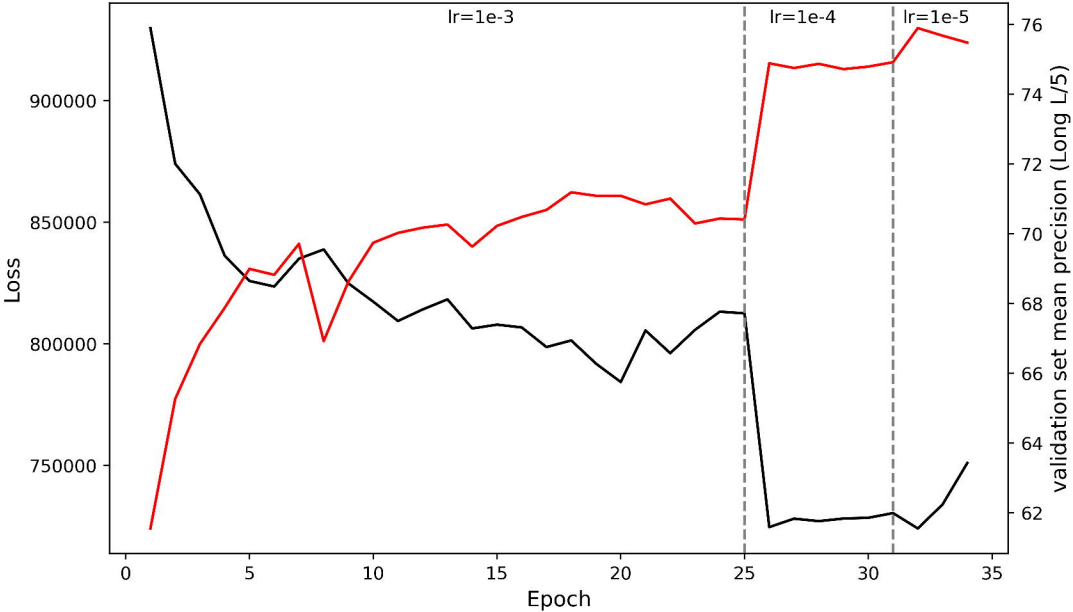
lr=1e-3
lr=1e-4
lr=1e-5
Loss
900000
850000
800000
750000
validation set mean precision (Long L/5)
76
74
72
70
68
66
64
62
0
5
10
15
20
25
30
35
Epoch

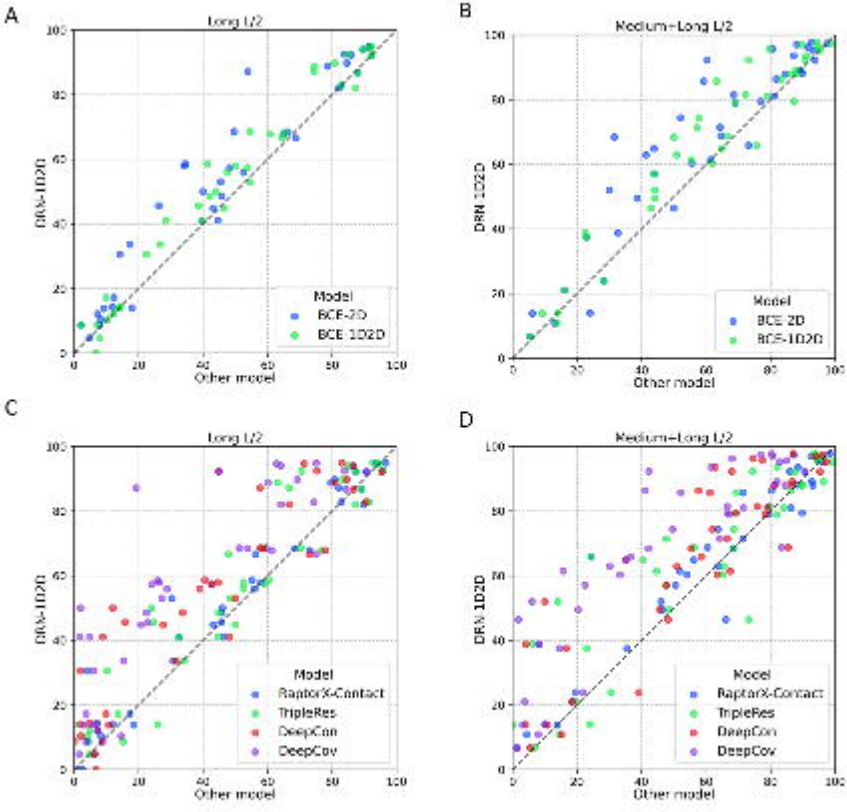
A
Long L/2
DRN-1D2D
Other model
Model
BCE-2D
BCE 1D2D
B
Medium+Long L/2
DRN 1D2D
Other model
Model
BCE 2D
BCE-1D2D
C
Long L/2
DRN-1D2D
Other model
Model
RaptorX-Contact
TripleRes
DeepCon
DeepCov
D
Medium+Long L/2
DRN 1D2D
Other model
Model
RaptorX-Contact
TripleRes
DeepCon
DeepCov

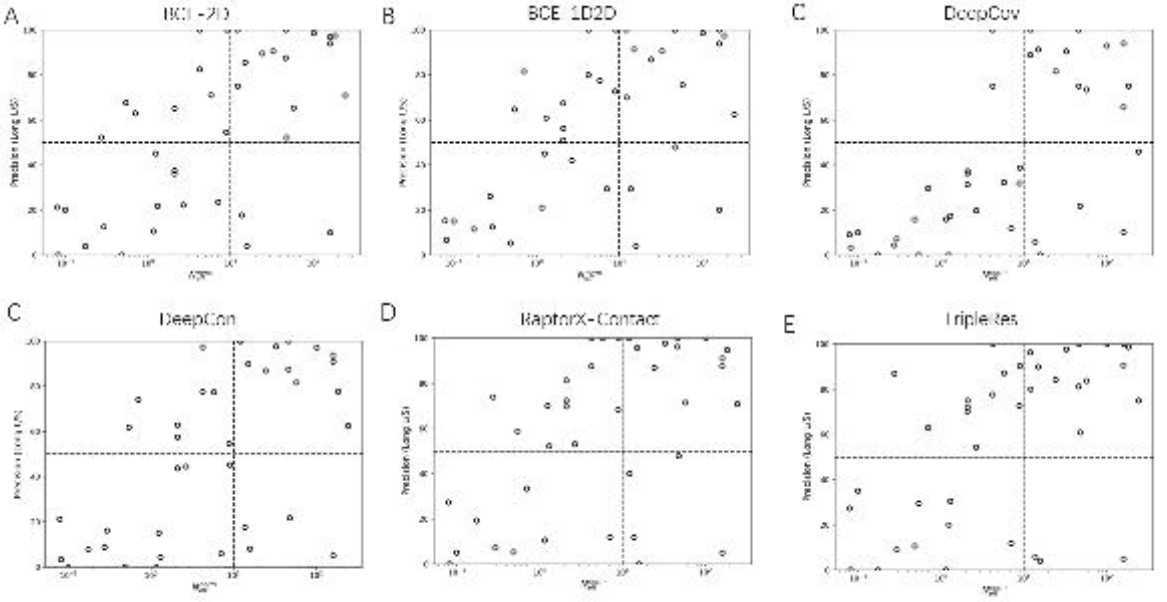
A
B
C
C
D
E
DeepCon
RaptorX-Contact
TripleRes